A Level Set Method to Image Segmentation Based on Local Direction Gradient

Yanjun Peng[1], Yingran Ma[1]
[1] College of Computer Science and Engineering, Shandong University of Science and Technology
Qingdao, 266590 - China
[e-mail: pengyanjuncn@163.com]
[e-mail: 707641531@qq.com]
*Corresponding author: Yanjun Peng

Received July 27, 2017; revised October 4, 2017; revised November 19, 2017; accepted December 5, 2017; published April 30, 2018

Abstract

For image segmentation with intensity inhomogeneity, many region-based level set methods have been proposed. Some of them however can't get the relatively ideal segmentation results under the severe intensity inhomogeneity and weak edges, and without use of the image gradient information. To improve that, we propose a new level set method combined with local direction gradient in this paper. Firstly, based on two assumptions on intensity inhomogeneity to images, the relationships between segmentation objects and image gradients to local minimum and maximum around a pixel are presented, from which a new pixel classification method based on weight of Euclidian distance is introduced. Secondly, to implement the model, variational level set method combined with image spatial neighborhood information is used, which enhances the anti-noise capacity of the proposed gradient information based model. Thirdly, a new diffusion process with an edge indicator function is incorporated into the level set function to classify the pixels in homogeneous regions of the same segmentation object, and also to make the proposed method more insensitive to initial contours and stable numerical implementation. To verify our proposed method, different testing images including synthetic images, magnetic resonance imaging (MRI) and real-world images are introduced. The image segmentation results demonstrate that our method can deal with the relatively severe intensity inhomogeneity and obtain the comparatively ideal segmentation results efficiently.

Keywords: image segmentation, image gradient, level set method, intensity inhomogeneity

1. Introduction

Image segmentation plays an important role in computer vision. Its aim is to classify an image into different regions based on intensities, colors and textures, etc. Because of the imperfection of imaging devices or illumination variations, the phenomenon of intensity inhomogeneity and weak edges often occurs in real-world images and medical images, which may bring several difficulties to the image segmentation methods. So, it is impossible to segment objects in images properly, according to the assumption that each object region has uniform intensity.

In recent years, various image segmentation models based on level set methods have been proposed, which can be classified into two main categories: edge-based models and region-based models. A classical edge-based model is the snake model [1]. Following it, many improved models have been proposed, such as geodesic/geometric active contours [2, 3]. To prevent the active contours from trapping into the local minimum, Bresson et al. [4, 5] introduced a fast global active contour/snake model. For region-based models, the most well-known one is the Mumford-Shah (MS) model [6], which assumes that the image intensity is piecewise smooth and can segment images with intensity inhomogeneity. However, because of its unknown contours and non-convexity of the problem, it is difficult to minimize its energy functional. So, its simplified models, such as Chan-Vese (CV) model [7] and the PS model [8] have been proposed, which based on level set method to represent the evolving curve. Nevertheless, CV model is not suitable to images with intensity inhomogeneity because it demands for an approximation of a given image with a two-phase piecewise constant representation. Although PS model can deal with intensity inhomogeneity of the images properly, but the process of solving two partial differential equations is complicated and time-consuming. For more systematical introduction about the related methods, one can refer to [9].

Another important aspect of dealing with images with intensity inhomogeneity is local region-based level set method. The well-known local binary fitting (LBF) model [10] introduces the local region mean information into the CV model. Later in [11], Li et al. proposed the local intensity clustering (LIC) method with the help of a bias field to cope with intensity inhomogeneity preferably. After that, for better estimation of the bias field and segmentation of MRI, an optimization process of multinomial coefficients is adopted in [12]. Another local region-based level set method is local region model (LRB) [13] whose three different internal energy measures are introduced in local region, including the uniform modeling energy, the means separation energy and the histogram separation energy. Following that, local region means and variances are used in [14] to interpret the MS model. Recently, in [15], Zhang et al. presented a novel statistical level set method with local Gaussian distributions and maximum likelihood method, which can estimate the piecewise constant image and the bias field more precisely.

The major characteristics of the models mentioned above is that they all utilize the local mean information or local distribution of image intensity with the help of the bias field of intensity inhomogeneity, but not fully employ the information of image gradient. Whereas, the image gradient plays an important role in segmentation of images with low contrast, weak edges and intensity inhomogeneity, etc. In this paper, we propose a novel variational level set method combined with local direction gradient information which explores the

relationships between segmentation objects and the different direction gradients of a pixel and also integrate local spatial information to improve its anti-noise ability.

In addition, keeping numerical stability is necessary and essential in implementing the level set methods, which implies that the corresponding level set function (LSF) can't be very flat or steep near the zero level set. The traditional approaches initialize the LSF to be a signed distance function (SDF), but this will not last during curves evolution. A remedy measure called re-initialization periodically keeping the degraded LSF being an SDF. Among many re-initialization methods [16-18], the most frequently used is proposed by Sussman et al. [17], which iteratively solves a re-initialization partial differential equation. However, when the LSF is far away from an SDF, this method fails to yield a desirable SDF. Besides, the frequency of re-initialization is totally determined by one's experience and experiments. Lately, several variational level set formulations [19-21] have been presented to regularize the LSF during evolution, which eliminate the re-initialization procedure. The most widely adopted model is proposed by Li et al. [19], which introduces a distance regularized term into energy function of the corresponding model. Later in [15], Zhang et al. remark that those distance regularized terms may produce some unnecessary valleys and peaks and make level set evolution easy to fall into some local minima. So in [22], a novel reaction-diffusion method is introduced into level set evolution to obtain a stable numerical solution and to ensure the boundary antileakage. Moreover, this diffusion term has been applied in [15] successfully.

Considering the superiority of the diffusion term mentioned above, we integrate it into our model with an edge indicator function not only because the time-consuming re-initialization procedure can be completely eliminated with the diffusion term but also the pixels in homogeneous regions can be classified correctly irrespective of the LSF initialization.

To sum up, the core idea of the proposed method is to utilize the image gradient information to cope with intensity inhomogeneity. Firstly, based on two assumptions about intensity inhomogeneity, we consider it as a linear attenuation of gray value in local image regions and induce a new classification method with the weight of Euclidean distance. Secondly, image gradients in the directions to local minimum and maximum around a pixel and variational level set method with spatial neighborhood information are used to overcome the image noise partly. Thirdly, the diffusion term with an edge indicator function are combined to classify the pixels in homogeneous regions and ensure stability of numerical implementation and boundary antileakage.

2. Linear Attenuation of Image Gray Value

The intensity inhomogeneity is usually viewed as image decomposition model, where it is attributed to a component of an image. The following multiplicative model is widely adopted in many papers [11, 15, 23].

$$I = bJ + n \tag{1}$$

where J represents the true image which is a piecewise constant; b is the component that accounts for the intensity inhomogeneity, and also the image intensity bias field; n is additive noise and can be assumed to be zero-mean Gaussian model.

Contrast with piecewise constant model, there are two assumptions on J and b as described in many papers [11, 23, 24]. We summarize these as follows:

(A1) The true image J characterizes a physical property of the object being considered, which has the same value for the pixels on the same type of object.

(A2) The bias field b is varying slowly, which means that it can be modeled by a piecewise linear approximation in the local region.

Based on the model in (1) and considering assumptions (A1) and (A2), we present the linear attenuation of gray value in local region image with intensity inhomogeneity, and then induce a new pixel classification method.

Suppose the phenomenon of intensity inhomogeneity results from different illuminants in the image, and the light intensity of one point decays linearly in the Euclidean distance from illumination. So, the **Fig. 1** shows the linear attenuation of gray value in local region of the image with intensity inhomogeneity.

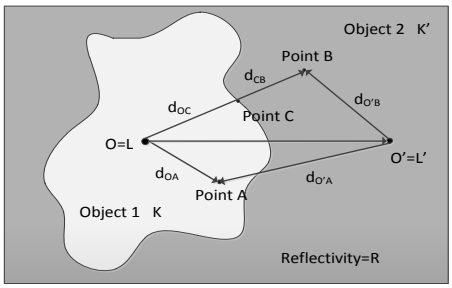

Fig. 1. Linear attenuation of gray value in local region of the image. There are two objects: target and background with two illuminants, O and O' respectively. Suppose they have the same reflectivity R but different linear decay rates: k and k', and the illumination intensity of the two illuminants are L and L' respectively.

Based on **Fig. 1** and the corresponding definitions, gray values of any pixels in local region can be obtained, e.g. the gray values of point O, O', A and B can be calculated as follows

$$I_O = LR, \qquad I_{O'} = L' R,$$
$$I_A = RL_A = R(L - kd_{OA}), \quad I_B = RL_B = R(L - kd_{OB}) \tag{2}$$

Relying on formula (2), we consequently create synthetic images with different locations, intensities and linear decay rates of illuminants which are shown in **Fig. 2**.

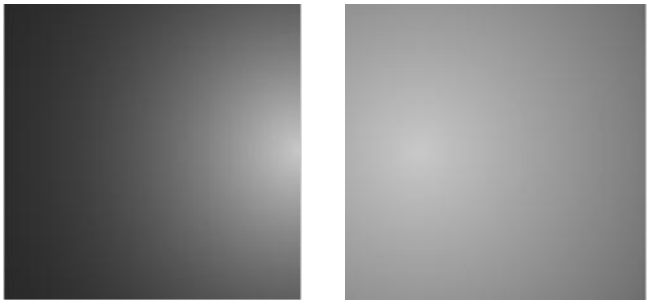

Fig. 2. Synthetic images with linear decay of grey value. Left: decay rates $k = 0.84$, intensity of the illuminant $I_O = 220$. Right: decay rates $k = 0.5$, intensity of the illuminant $I_O = 250$.

Subsequently, in order to classify pixels shown in **Fig. 1**, we explore the gray value changing rates of one pixel to the two illuminants with the Euclidean distance in the image domain. E.g. considering formula (2), the changing rates of the point B in the **Fig. 1** can be expressed through the following formulas

$$\frac{|I_O - I_B|}{d_{OB}} = \frac{|I_O - (L'R - k'Rd_{O'B})|}{d_{OB}} = \frac{|I_C + Rkd_{OC} - (L'R - k'Rd_{O'B})|}{d_{OC} + d_{CB}} = \frac{|I_C - L'R + Rkd_{OC} + Rk'd_{O'B}|}{d_{OC} + d_{CB}} \tag{3}$$

$$\frac{|I_{O'} - I_B|}{d_{O'B}} = \frac{|L'R - L'R + Rk'd_{O'B}|}{d_{O'B}} = Rk' \tag{4}$$

where d_{OB} and $d_{O'B}$ are the Euclidean distance of point B to the two illuminants O and O' respectively; point C is the crossing point of the boundary of target and joint line between O and B; the definition of other variables is the same as in formula (2). To compare formula (3) and (4), formula (4) is modified as follows.

$$\frac{|I_{O'} - I_B|}{d_{O'B}} = Rk' = \frac{|Rk'd_{OC} + Rk'd_{CB}|}{d_{OC} + d_{CB}} \tag{5}$$

Moreover, considering the assumptions (A1), (A2), and **Fig. 1** is confined to the local region of images, the following conditions are satisfied

$$k \approx k',\ d_{O'B} \approx d_{CB},\ |I_C - I_{O'}| >> 0 \tag{6}$$

where $k \approx k'$ means the linear decay rates of different objects are similar in the local region; it is the same with $d_{O'B} \approx d_{CB}$; $|I_C - I_{O'}| >> 0$ denotes that the gray value of target boundary point is quite different from background illuminants, which is the main difference of gray values between two objects in the image.

Substituting formula (6) into (3) and (5), we can obtain the following expression.

$$\frac{|I_{O'} - I_B|}{d_{O'B}} < \frac{|I_O - I_B|}{d_{OC} + d_{CB}} \tag{7}$$

This expression can be explained with the **Fig. 1** where the variance rate of gray value from illuminant O' of the object 2 to the unclassified point B should be smaller than from O, the illuminant of the object 1. One can use this quantity relation to classify the point B, i.e. it should belong to the same classification with the illuminant O', which is the same situation for the point A. Based on this conclusion, this paper proposes a new pixel classification method to deal with images with intensity inhomogeneity which will be introduced in the next section.

3. The proposed method

This section describes the details of proposed method based on variational level set method and the diffusion process to level set function.

3.1 A New Classification Method Combined with Weights of Euclidian Distance

Based on the conclusion obtained from formula (7), the new classification method combined weightings of Euclidian distance is presented. Considering two-phase image segmentation problem, let Ω_1 and Ω_2 represent the target region and background region respectively. The formula (7) can be generalized through the following expression

$$X \in \Omega_i \Leftrightarrow \frac{|\Delta I_{X \to O_i}|}{d_{X \to O_i}} = \min\left\{\frac{|\Delta I_{X \to O_j}|}{d_{X \to O_j}}\right\},\ s.t.\ O_i \in N(X),\ i, j = 1, 2 \tag{8}$$

where X is one pixel in image; O_i is the location of illuminant of i-th segmentation object in the local region of X, denoted as $N(X)$; $\Delta I_{X \to O_i} = I_X - I_{O_i}$ is the gray value difference of the point X to the i-th illuminant O_i; $d_{X \to O_i}$ is the Euclidian distance from X to O_i.

Using minimum quadratic multiplication in expression (8), the objective function of the proposed method can be defined as follows

$$F_{\min} = \sum_{i=1}^{2} \sum_{j=1}^{N} \frac{(I(X_j) - I(O_i))^2}{d^2(X_j, O_i)} u_i(X_j), \quad s.t.\ O_i \in N(X_j) \tag{9}$$

where u_i is the indicator function or membership function of the region Ω_i to be determined, i.e. $u_i(X) = 1$ for $X \in \Omega_i$ and $u_i(X) = 0$ for $X \notin \Omega_i$; N is the number of elements. The meaning of the other variables is the same with formula (8).

It is worth mentioning that the difference between the proposed objective function (8) with of fuzzy C-means (FCM) clustering is the new introduced clustering centers which are spatially varying with Euclidian distance from the unclassified elements to the corresponding local illuminants.

If the locations of local illuminants to the untreated pixels i.e. $d^2(X_j, O_i)$ are known, the problem (8) is similar with FCM. But when they are all uncertain, it becomes a NP-hard problem, which every pixel in local region of point X is possible illuminant making it impossible to solve the problem (8). However, considering this is two-phase image segmentation problem, the gray value of every pixel can be acquired in two aspects: increasing from the minimum gray value of pixel and decreasing from the maximum gray value of pixel in local region. In this way, (8) compares the two absolute values of changing rate in the directions of minimum and maximum illuminant locations and selects the minimum as the corresponding classification to which the unclassified pixel belongs. The process is illustrated in **Fig. 3**.

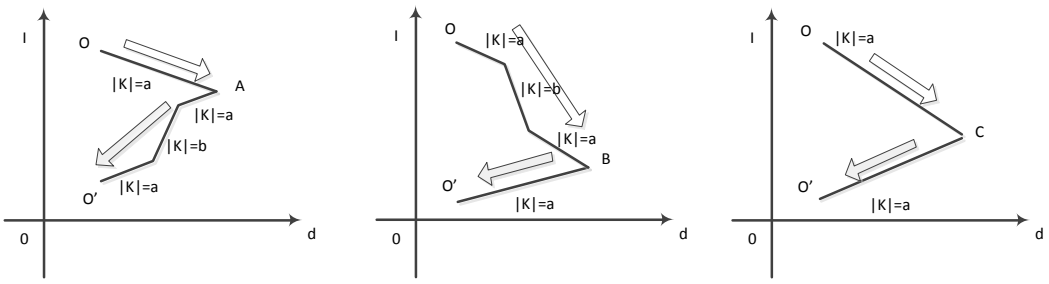

Fig. 3. Three different situations of absolute values of changing rate. O and O' are the maximum and minimum gray value in the local region respectively. Left: the point $A \in \Omega_1$. Middle: the point $B \in \Omega_2$. Right: the classification of point C is uncertain.

In **Fig. 3**, the first two situations are easy to classify, according to the minimum of absolute values of changing rate. However, in the rightmost situation, only with the information of changing rates, it is impossible to classify the point C correctly, which brings challenge to our method. Fortunately, with the help of diffusion process of level set function described in the section 3.3, the right situation can be handled properly.

3.2 Variational Level Set Method with Spatial Information

To implement the problem (9), variational level set method is adopted in our method. With the help of level set function ϕ and its Heaviside function $H(\phi)$, the indicator functions are presented as follows

$$\begin{cases} M_1(X) = H(\phi(X)) \\ M_2(X) = 1 - H(\phi(X)) \end{cases} \tag{10}$$

By replacing $u(X)$ in (9) with (10), the data term of our proposed method is shown as below

$$\begin{aligned} E(\phi) &= \int_{\Omega} \frac{(I(X) - I(O_1))^2}{d^2(X, O_1)} M_1(\phi) \mathrm{d}X + \int_{\Omega} \frac{(I(X) - I(O_2))^2}{d^2(X, O_2)} M_2(\phi) \mathrm{d}X \\ &\textit{subject to } I(O_1) = \min(N_X),\ I(O_2) = \max(N_X),\ \mathrm{N_X} = \left\{ Y \middle\| Y - X \right| < \rho \right\} \end{aligned} \tag{11}$$

where N_X is a neighborhood pixel set of point X with the radius ρ; O_1 and O_2 represent the location of minimum and maximum in N_X respectively. Note that when $\rho = 2$, the local region area of the point X becomes 8-connected, and the proposed method utilizes equivalently the direction gradient information of images.

However, because of the usage of image gradient information, model (11) is very sensitive to image noise. To overcome that, spatial information of image is widely employed by many methods [25, 26, 27]. In consequence, model (11) is improved by introducing spatial information of images in this paper.

Considering one unclassified point X in image domain, whose neighborhood pixel set is defined as $\varphi_X = \{Y \| Y - X| < \varepsilon\}$, the modified data term with spatial information is presented as follows

$$\begin{aligned} F_X(\phi) &= \sum_{i=1}^{2} \int_{\varphi_X} \frac{(I(Y) - I(O_i))^2}{d^2(Y, O_i)} M_i(\phi(X)) \mathrm{d}Y \\ &\textit{subject to } I(O_1) = \min(N_Y),\ I(O_2) = \max(N_Y),\ N_Y = \{Z \| Y - Z| < \rho\} \end{aligned} \tag{12}$$

model (12) implies that the classification of the point X depends on the neighborhood information, which enhances anti-noise capability of the proposed method. Parameter ε determines the smoothness of segmentation results.

Through extending the model (12) to entire image domain and introducing a truncated Gaussian function $K(X,Y)$ to denote the neighborhood relationship of point X and Y, the final data term of the proposed method is shown below

$$\begin{aligned} E(\phi) &= \int_{\Omega} \left(\sum_{i=1}^{2} \int_{\Omega} K(X,Y) \frac{(I(Y) - I(O_{iY}))^2}{d^2(Y, O_{iY})} M_i(X) \mathrm{d}Y \right) \mathrm{d}X \\ &\textit{subject to } I(O_{1Y}) = \min(N_Y),\ I(O_{2Y}) = \max(N_Y),\ N_Y = \{Z \| Y - Z| < \rho\} \end{aligned} \tag{13}$$

where

$$K(X,Y) = \begin{cases} \dfrac{1}{a} e^{-|Y-X|^2/2\sigma^2} & |Y - X| < \delta \\ 0 & \text{otherwise} \end{cases}, \quad \textit{subject to } \int K(X,Y) = 1$$

a is a normalization constant such that $\int K(X,Y) = 1$, σ is the standard deviation of the Gaussian function, and δ is the radius of the neighborhood, which is different with ρ.

3.3 Diffusion Process of Level Set Function

To keep numerical stability, it is necessary to characterize the level set from a signed distance function during the iteration. The most widely used method is the signed distance regularization formula which is proposed by Li et al. [19]. However, Zhang et al. [15] indicate that it generates some unnecessary valleys and peaks, which makes level set evolution easy to fall into some local minima. In [22], the diffusion process to level set evolution is first applied to make it reinitialization-free and boundary antileakage. The energy function of diffusion is shown as follows

$$F_\mu = \frac{1}{2}\mu\int_\Omega |\nabla\phi|^2 \mathrm{d}x \tag{14}$$

whose gradient flow is

$$\begin{cases} \phi_t = \mu\Delta\phi, \quad x \in \Omega \subset R^n \\ subject\ to\ \phi(x, t=0, \mu) = \phi_0(x) \end{cases} \tag{15}$$

In this paper, we apply diffusion process to level set function to segment the pixels in the homogeneous regions which is demonstrated in **Fig. 3**, without considering the manner of level set initialization, i.e. “out positive in negative” or “out negative in positive”. The function of diffusion process in this paper can be illustrated in **Fig. 4**.

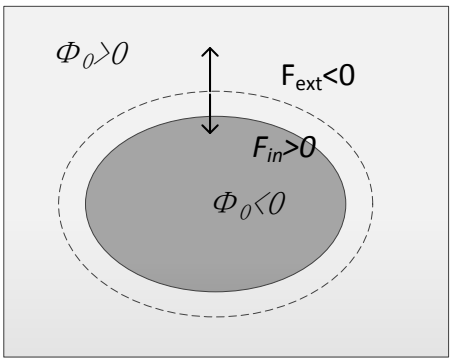

Fig. 4. The contradiction of the internal force and external force around the background boundary only with length term.

In **Fig. 4**, length term is considered whose corresponding internal force will be opposite to the external if it is negative around the background boundary. In this case, the homogeneous regions in the oval target will be classified correctly, i.e. $\phi > 0$ with the internal force $F_{in} > 0$. But the homogeneous region in the background will be misclassified. The evolving curve will stop at somewhere around the target boundary because of the opposite direction of F_{in} and F_{ext}, making it hard to obtain the correct segmentation results.

With the diffusion process to level set function, the homogeneous regions can also be classified correctly with only edge information of images. However, in [22], the parameter μ should be smaller than its upper limit, i.e. 0.25 to prevent boundary leakage and it is all the same value to entire image domain without considering the image data. So, in this paper, we introduce an edge indicator function to dynamically adjust μ according the gradient information, i.e. μ becomes larger in flat regions and smaller around edges. The improved diffusion term is presented as follows

$$F_g = \frac{1}{2}\mu g(x)\int_\Omega |\nabla\phi|^2 \mathrm{d}x \tag{16}$$

where $g(x)$ is an edge indicator function which is shown below

$$g(x) = \frac{1}{1+(r/K)^p}, \quad s.t.\ p = 1,2 \tag{17}$$

In conclusion, combining (13) and (16), the energy function of our method is defined as

$$\begin{aligned} E(\phi) &= \int_\Omega \Big(\sum_{i=1}^{2} \lambda \int_\Omega K(X,Y)\frac{(I(Y)-I(O_{iY}))^2}{d^2(Y,O_{iY})} M_i(X)\mathrm{d}Y\Big)\mathrm{d}X + \frac{1}{2}\mu g(X)\int_\Omega |\nabla\phi|^2 \mathrm{d}X \\ &\textit{subject to}\ \ I(O_{1Y}) = \min(N_Y),\ \ I(O_{2Y}) = \max(N_Y),\ \ \mathrm{N_Y} = \{\mathrm{Z} \big| |Y-Z| < \rho\} \end{aligned} \tag{18}$$

where λ is the weight parameter of data term which is set by the extent of intensity inhomogeneity of the images. To minimize this energy functional, its gradient flow is used as the level set evolution equation in the proposed method. By solving the gradient flow equation

$$\frac{\partial\phi}{\partial t} = -\frac{\partial E}{\partial\phi} \tag{19}$$

the corresponding gradient flow equation as

$$\frac{\partial\phi}{\partial t} = \delta_\varepsilon(\phi)\left[\lambda\int_\Omega K(X,Y)\frac{(I(Y)-I(O_{2Y}))^2}{d^2(Y,I(O_{2Y}))}\mathrm{d}Y - \lambda\int_\Omega K(X,Y)\frac{(I(Y)-I(O_{1Y}))^2}{d^2(Y,I(O_{1Y}))}\mathrm{d}Y\right] + \mu g(X)\Delta\phi \tag{20}$$

where δ_ε is the derivative of a Heaviside function H_ε which is defined by

$$H_\varepsilon(x) = \frac{1}{2}\left[1+\frac{2}{\pi}\arctan(\frac{x}{\varepsilon})\right] \qquad \delta_\varepsilon = H'_\varepsilon(x) = \frac{1}{\pi}\frac{\varepsilon}{\varepsilon^2+x^2} \tag{21}$$

In addition, the data term in (20) can be expressed in convolution type

$$\frac{\partial\phi}{\partial t} = \delta_\varepsilon(\phi)\left[\lambda K(X) * \frac{(I(Y)-I(O_{2Y}))^2}{d^2(Y,I(O_{2Y}))} - \lambda K(X) * \frac{(I(Y)-I(O_{1Y}))^2}{d^2(Y,I(O_{1Y}))}\right] + \mu g(X)\Delta\phi \tag{22}$$

Finally, the diffusion term in (22) can be implemented by the following formula after each iteration in a splitting scheme [15].

$$\phi^{l+1} = \phi^l + \Delta t\cdot\nabla^2\phi^l \tag{23}$$

where ∇^2 represents the Laplacian operator. The ϕ^{l+1} can also be approximated by $\phi^{l+1} = K * \phi^l$, where K is either a Gaussian Kernel or a constant kernel, and Δt represents the diffusion strength, i.e. $\Delta t = \mu g(X)$ in this paper.

At last, the whole arithmetic explanation of our method is listed in Algorithm 1 as follows.

Algorithm 1. The whole steps of the proposed method

Input: The image needs to be segmented

Output: The converged level set function as the segmentation result

Step 1: Initialize the parameters, i.e. ρ, λ, σ, δ, t, μ properly

Step 2: Initialize the level set function ϕ, i.e. "out positive in negative" or "out negative in positive" according to the image actual situation

Step 3: Calculate the external force of the evolving curve, i.e. F_{in}, using the first term of the formula (20)

Step 4: Execute the filtering operation in F_{in}, using the given kernel K in formula (13)

Step 5: Calculate the internal force of the evolving curve, i.e. F_{out}, using the second term of the formula (20)

Step 6: Calculate the gradient flow of the level set function ϕ, according to the formula (20)

Step 7: Update ϕ using formula (23) as current iteration

Step 8: Judge whether the iterative process is over. If it's not, go to step 3. Otherwise the current level set function ϕ represents the final segmentation result.

4. Numerical Experiments

In this section, several numerical experiments on synthetic images, MRI and real images are implemented successively to verify effectiveness and efficiency of the proposed method. Although several parameters are involved in our method, the choice of these parameters is not difficult. Some of them, such as parameters t and μ, can be fixed as $t = 0.1$ and $\mu = 0.25$, i.e. its upper bound according to [21]. It is necessary to test the influence of different values of parameter ρ in (18) on the segmentation results. **Fig. 5** exhibits three segmentation results of the image of desert with three different values of ρ, i.e. 3, 7 and 11. From the segmentation results, one may draw a conclusion that the parameter ρ is just like the scale parameter of segmentation result. But with it increasing, the accuracy of segmentation results will reduce, partly because the condition (6) is no longer satisfied with the larger local regions, i.e. the larger value of parameter ρ in (18). So, unless otherwise mentioned in the next experiments, the parameter ρ is fixed as $\rho = 3$ in the most of cases.

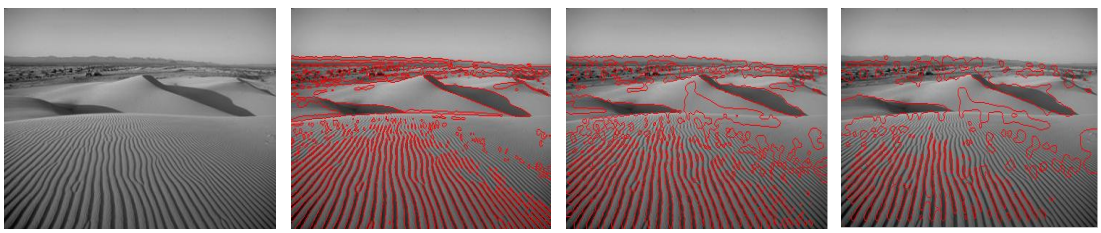

(a) (b) (c) (d)

Fig. 5. The influence of different values of ρ on the final segmentation results. (a) the input desert

image. (b) $\rho = 3$. (c) $\rho = 7$. (d) $\rho = 11$.

The parameter λ of the data term in (22) determines the robustness to the intensity inhomogeneity in our method, i.e. the more severe of intensity inhomogeneity in images, the larger the parameter λ is to better capture the weak edges and details. But the segmentation results with larger λ are easily influenced by the noise in input images in practice. As for the values of parameter σ and δ in the kernel function in (13), they jointly decide the anti-noise capacity of the proposed model. Obviously, when they take larger values, the final evolution curves and segmentation results become more smoothness, probably at the cost of segmentation details and accuracy. So, there must be a tradeoff between the robustness to the intensity inhomogeneity (λ in (18)) and to the image noise (σ and δ in (13)). In experimental practice, the λ can be set in the range of 1~10. $\sigma = 1 \sim 2$ and $\delta = 3,5$ based on the actual situation. The diffusion term in (22) can be implemented with a kernel filtering template K which is defined below to approximate the Laplacian operator $\nabla^2 \phi$ by $K * \phi$.

$$K = \begin{pmatrix} 0 & 1 & 0 \\ 1 & -4 & 1 \\ 0 & 1 & 0 \end{pmatrix}$$

Therefore, the solution of the diffusion equation (23) can be discretized as follows

$$\phi^{l+1} = \phi^{l} * \begin{pmatrix} 0 & \Delta t & 0 \\ \Delta t & 1-4\Delta t & \Delta t \\ 0 & \Delta t & 0 \end{pmatrix} \tag{24}$$

where Δt is the time step of the diffusion process in two-step splitting method [22], i.e. $\Delta t = \mu g(X)$ in here. At last, our method is run on such platform: Intel Core i5 CPU, 3.30 GHz, 4 GB memory, and implemented by Matlab R2014a.

4.1 Results on Synthetic images

In this section, two classical edge-based model and region-based model: GAC [3] and CV [7] are implemented to compare the proposed method on two synthetic images with intensity inhomogeneity.

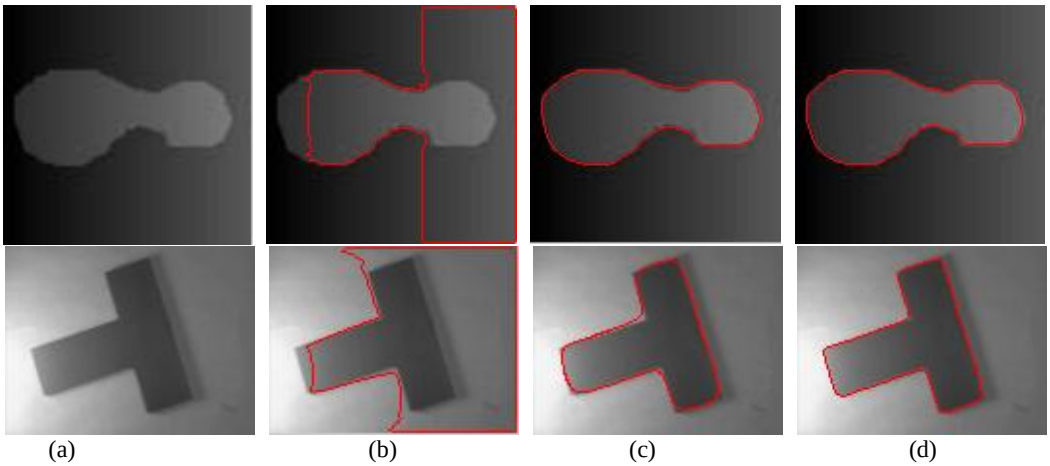

(a) (b) (c) (d)

Fig. 6. The influence of different values of ρ on the final segmentation results. (a) Input images. (b) CV model. (c) GAC model. (d) The proposed method.

From the segmentation results shown in **Fig. 6,** it can be seen that our method achieves satisfying results because we exploit local gradient information, which can better handle with intensity inhomogeneity. In contrast, CV model only utilizes global intensity means to segment object from background, and can't cope with intensity inhomogeneity. Although GAC model take advantage of image gradient information, which can deal with intensity inhomogeneity, but boundary leakage may occur in low contrast regions.

In the next experiment, to verify our method is robust to the initialization locations of the level set, we compare our method with the local image region information based methods, i.e. local region-based (LRB) level set methods [13] and local binary fitting (LBF) model [10]. **Fig. 7** demonstrates the segmentation results of a synthetic image with four different initialization locations of the level set. Form the results, it can be seen that because the LRB and LBF utilize the local information of the images, which make the level set evolution act locally. Therefore, the evolution can be easily trapped into local minima, although with the improved regularization of Dirac functional. And only get correct segmentation results with some specific initialization locations of the level set. However, with the help of local direction gradient information of images and diffusion process of level sets, our proposed method is robust to the initialization locations of the level set. In addition, due to the degree of intensity inhomogeneity in **Fig. 7** is relatively low the parameter λ of data term is set as 5.

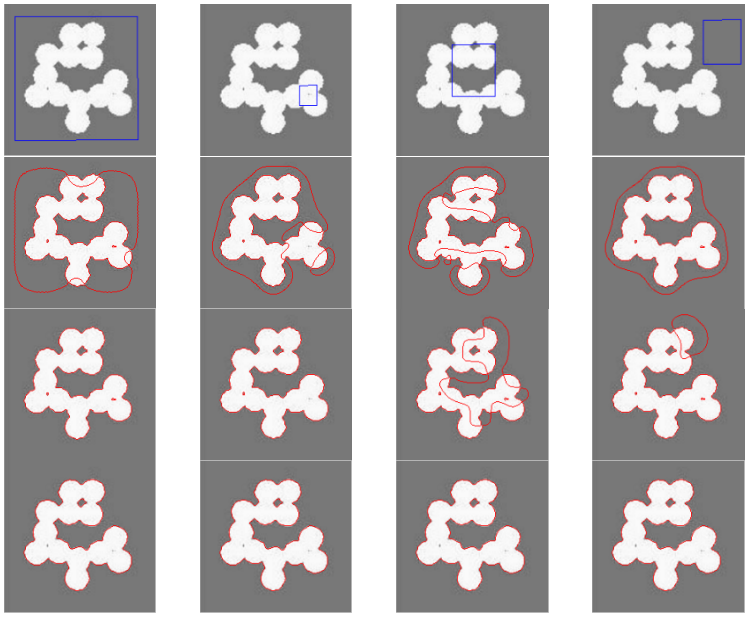

Fig. 7. Different initialization locations of level set and corresponding segmentation results. Top to bottom: different locations of level set initialization; results of the LRB model; result of the LBF model; result of the proposed method.

4.2 Stable Performance for Different Degrees of Intensity Inhomogeneity

In this section, several different types of human brain MRI images with different strength of intensity inhomogeneity are used, and the CV model [7], LRB model [13], LBF model [10], LIC model [11] and LGF model [15] are compared with our method.To quantitatively evaluate the performance of the competing methods, the Jaccard similarity (JS) [28] is used which is defined as

$$J(S_1, S_2) = \frac{|S_1 \cap S_2|}{|S_1 \cup S_2|} \times 100\% \tag{25}$$

where $|\cdot|$ represents the area of a region, S_1 is the region segmented by the algorithm and S_2 is the corresponding region in the ground truth. The closer the JS values to 1, the better the segmentation.

In the next experiment, we select human brain MRI images with relatively severe intensity inhomogeneity and weak edges. The brain MR images used here are from McGill BrainWeb: http://www.bic.mni.mcgill.ca/brainweb/. The segmentation results and corresponding JS values of white matter (WM) of different methods are shown in **Fig. 8** and **Table 1**. Note that in the following experiments, the background intensity is considered as zero by default. So, our purpose is to segment the images into two parts: grey matter (GM) and white matter.

From the segmentation result of CV model in **Fig. 8**, it can be seen that the intensity inhomogeneity of the MRI image is relatively severe. The **Table 1** shows that the result of LIC gets the best performance among these models, partly because it belongs to multiphase segmentation method which can better segment the three parts (i.e. WM, GM and background) in this image. And the bias correction technique is used which can improve its convergence speed. Our method is in the second place, but has a higher capacity of capturing the details of the image than local-region based models, especially in the low contrast areas with intensity inhomogeneity. Because the degree of intensity inhomogeneity in **Fig. 8** is relatively significant, the parameter of data term is set as 10.

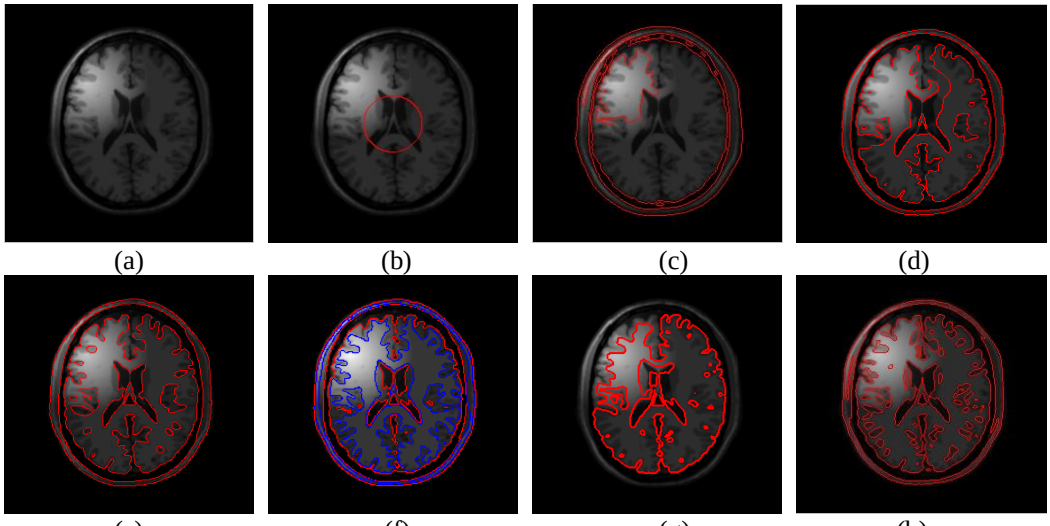

Fig. 8. Segmentation results of corresponding methods. (a) Input image. (b) Initialization of the level set function. (c) CV model. (d) LRB. (e) LBF. (f) LIC. (g) LGF. (h) The proposed method.

Table 1. Segmentation accuracy of white matter in **Fig. 8** with different methods

Models	CV	LRB	LBF	LIC	LGF	Our method
JS values of white matter in **Fig. 8**	20.67	83.23	86.21	**93.80**	85.68	89.19

Subsequently, in order to evaluate stable performance of our method for different degrees of intensity inhomogeneity, two groups of experiments are implemented where additional bias field are introduced artificially. In this paper, we use the coefficient of variations (CV)

[29] to quantify the degree of intensity inhomogeneity. We define CV for one tissue, gray matter or white matter (e.g. white matter in here) as

$$CV(T) = \frac{\sigma(T)}{\mu(T)} \times 100\% \tag{26}$$

where $\sigma(T)$ and $\mu(T)$ are the standard deviation and mean of the intensities in the tissue T.

For quantitative comparison, the resulting JS values of different methods in group one and two are listed in **Tables 2** and **3** respectively. And the corresponding JS of all these results are plotted in **Fig. 9** (a) and (b). The segmentation results with $CV = 60\%$ and $CV = 70\%$ in group one and two are shown in **Fig. 10** and **Fig. 11** respectively.

From **Fig. 9**, it can be seen that with the degree of intensity inhomogeneity increasing, the JS values of local region-based methods decline rapidly. However, due to take advantage of image direction gradient information, our method performs more stable than other methods. This can be concluded from **Fig. 10** and **Fig. 11**, where the proposed method can capture the edge information especially in the low contrast area. But our method has a limitation that the segmentation regions are not closed and continuous enough compared with region-based methods. This can be partly solved by introducing spatial information of the image according to the formula (12). At last, the parameter λ of data term is set as 15.

Table 2. Segmentation accuracy of white matter in group one with different degrees of intensity inhomogeneity.

CV (WM)	C-V	LRB	LBF	LIC	LGF	Our method
10%	80.80	84.01	87.16	**94.67**	90.32	91.07
20%	74.32	82.27	85.25	**92.92**	87.81	88.19
30%	68.45	78.78	81.77	**88.61**	86.39	86.16
40%	60.29	75.46	78.62	83.42	80.56	**85.27**
50%	50.97	70.42	75.31	78.35	76.60	**83.25**
60%	32.16	62.36	67.36	68.81	62.04	**80.52**
70%	26.49	55.39	58.32	61.55	52.29	**76.96**

Table 3. Segmentation accuracy of white matter in group two with different degrees of intensity inhomogeneity.

CV (WM)	C-V	LRB	LBF	LIC	LGF	Our method
10%	78.12	80.28	82.98	**90.72**	86.10	85.44
20%	70.72	75.36	76.15	**85.50**	82.78	83.81
30%	65.48	71.85	72.08	81.47	79.29	**82.67**
40%	50.19	60.77	63.64	70.09	68.54	**80.40**
50%	32.23	52.49	54.07	62.11	60.08	**78.88**

60%	20.82	39.47	40.66	53.83	52.67	**74.10**
70%	13.51	25.02	25.80	38.42	40.03	**70.90**

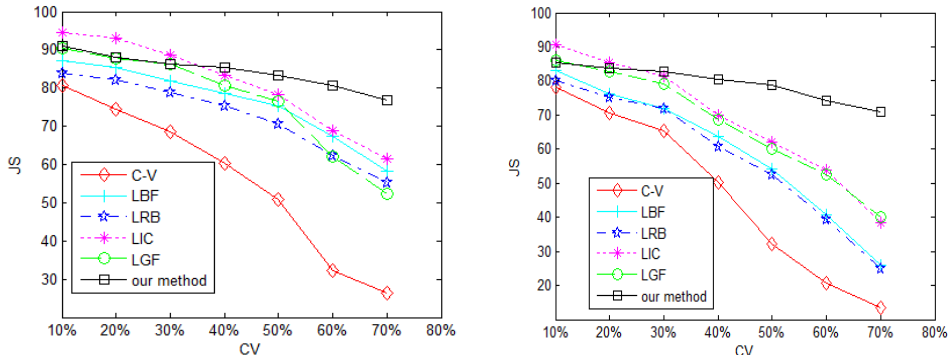

Fig. 9. the corresponding JS values of WM of two groups. (a) The first group. (b) The second group.

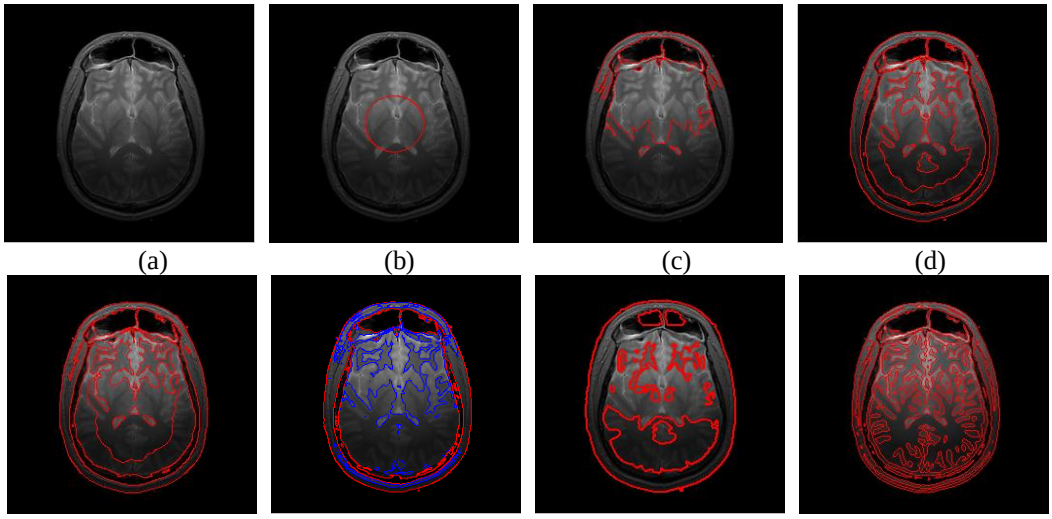

Fig. 10. Segmentation results of the first group with $CV = 60\%$. (a) Input image. (b) Initialization of the level set function. (c) CV model. (d) LRB. (e) LBF. (f) LIC. (g) LGF. (h) The proposed method.

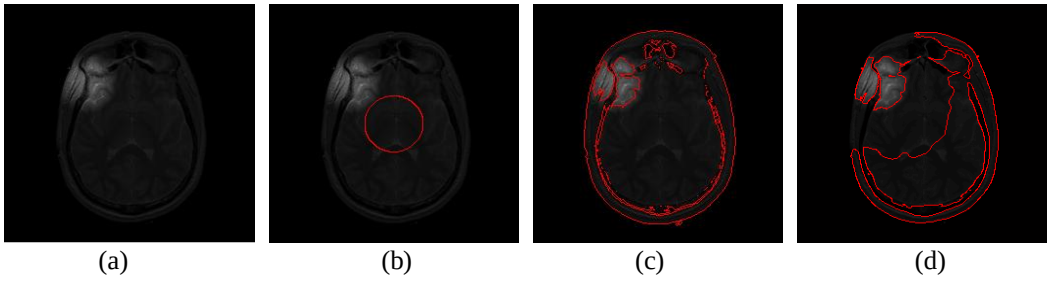

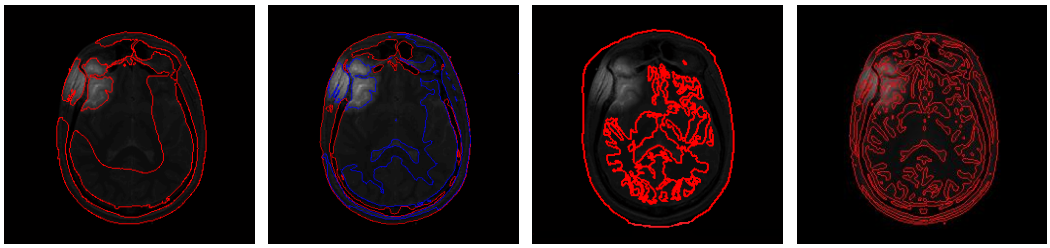

(e) (f) (g) (h)

Fig. 11. Segmentation results of the second group with $CV = 70\%$. (a) Input image. (b) Initialization of the level set function. (c) CV model. (d) LRB. (e) LBF. (f) LIC. (g) LGF. (h) The proposed method.

4.3 Results on Real Images

In this section, two real images are selected to verify the efficiency of our method. The segmentation results of the different methods are presented in **Fig. 12**. The iteration number and CPU time are listed in **Table 4.**

Fig. 12 and **Table 4** show that our method can get desirable segmentation results in an efficient way. The computation complexity of our method is about $O(\rho MN + 9n \times MN)$ of which the first part is the computational cost of data term and the second part is the diffusion process of level set function, where n is the number of iteration and M, N are the size of segmentation image. In comparison, because the LIC model and LGF model can be applied to simultaneous segmentation and bias correction, the computational cost should be higher than the methods which are capable of image segmentation only, i.e. CV model, LRB model, LBF model and our method. Note that, because the average intensity of segmentation objects is lower than the background in **Fig. 12**, the level set function of all models in here can be initialized with the "negative out positive in" for efficiency. For bird image, the 3-D view of data term of our method and the convergence properties of these six segmentation methods are shown in **Fig. 13** (a) and (b) respectively.

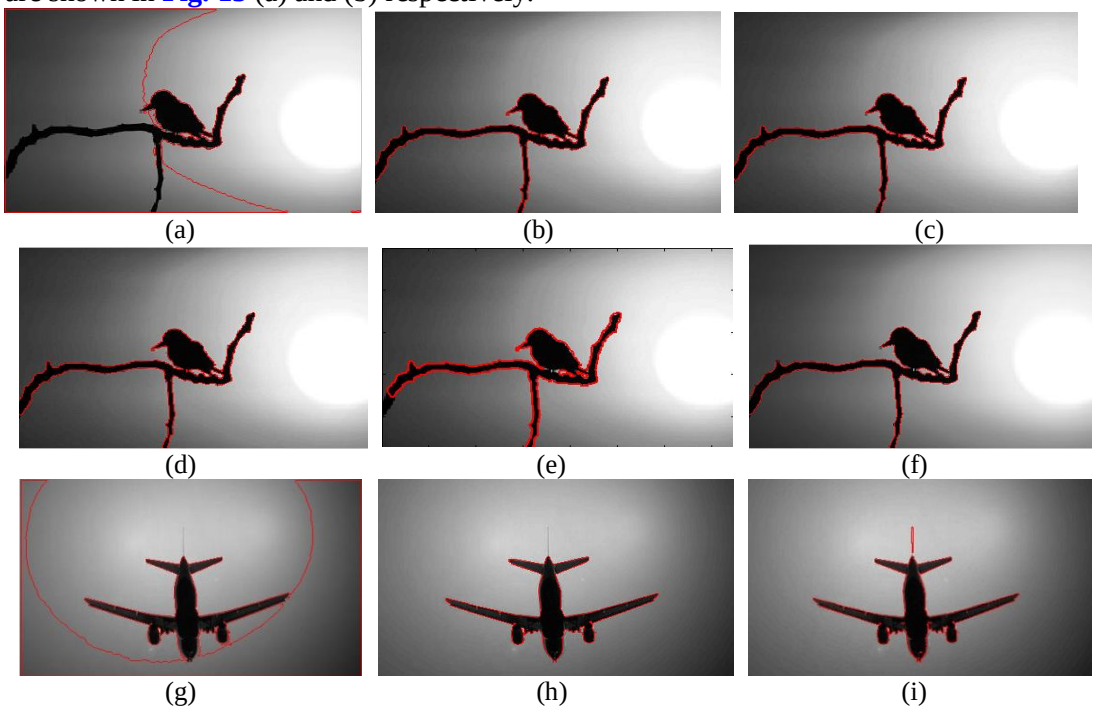

(a) (b) (c)

(d) (e) (f)

(g) (h) (i)

(j) (k) (l)

Fig. 12. Segmentation results of the two real images. (a) and (g) CV. (b) and (h) LRB. (c) and (i) LBF. (d) and (j) LIC. (e) and (k) LGF. (f) and (l) The proposed method.

Table 4. The iteration number and CPU time of **Fig. 12** with different methods.

Fig. 12	Models	CV	LRB	LBF	LIC	LGF	Our method
Bird	The iteration number	100	50	50	500	500	30
	CPU time (s)	2.58	5.62	6.14	25.40	28.39	4.50
Airplane	The iteration number	150	100	100	800	800	50
	CPU time (s)	3.42	8.96	9.42	38.27	45.52	6.72

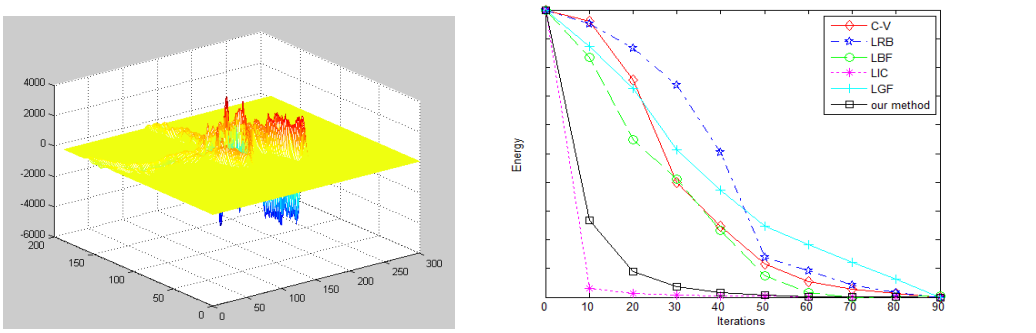

Fig. 13. Left: the 3-D view of data term of our method. Right: the convergence properties of these six segmentation methods

5. Conclusion

In this paper, we presented an image segmentation method based on direction gradient information which can deal with images with relatively severe intensity inhomogeneity and weak edges. To implement this method, the level set method with spatial neighborhood information is introduced to get the comparatively closed segmentation regions. In addition, with the help of the edge-based diffusion process of the level set function, the pixels in homogeneous regions of the same object in images can be classified correctly. Compared with some relevant level set based approaches, our method can get relatively efficient and ideal segmentation results, especially dealing with low contrast and weak edges in images. However, because our method is essentially a hard classification and two-phase segmentation method, one of the future research directions will be to extend the proposed method to soft classification and multi-phase segmentation.

References

[1] M. Kass, A. Witkin, and D. Terzopoulos, "Snakes: Active contour models," *International Journal of Computer Vision*, vol. 1, no. 4, pp. 321-331, January, 1988. Article (CrossRef Link)

[2] V. Caselles, F. Catte, T. Coll, and F. Dibos, "A geometric model for active contours in image processing," *Numerical Mathematics*, vol. 66, no. 1, pp. 1-31, December, 1993. Article (CrossRef Link)

[3] V. Caselles, R. Kimmel, and G. Sapiro, "Geodesic active contours," *International Journal of Computer Vision*, vol. 22, no. 1, pp. 61-79, February, 1997. Article (CrossRef Link)

[4] X. Bresson, S. Esedoglu, P. Vandergheynst, J.-P. Thiran, and S. Osher, "Fast global minimization of the active contours/snake model," *Journal of Mathematical Imaging and Vision*, vol. 28, no. 2, pp. 151-167, June, 2005. Article (CrossRef Link)

[5] X. Bresson, S. Esedoglu, P. Vandergheynst, J.-P. Thiran, and S. Osher, "Global minimizers of the active contour/snake model," in *Proc. of UCLA CAM Report*, January, 2005. Article (CrossRef Link)

[6] D. Mumford and J. Shah, "Optimal approximations by piecewise smooth functions and associated variational problems. Commun," *Pure Appl. Math*, vol. 42, no. 5, pp. 577-685, July, 1989. Article (CrossRef Link)

[7] T. F. Chan and L. A. Vese, "Active contours without edges," *IEEE Transactions on Image Process*, vol. 10, no. 2, pp. 266-277, February, 2001. Article (CrossRef Link)

[8] L. A. Vese and T. F. Chan, "A multiphase level set framework for image segmentation using the Mumford and Shah model," *International Journal of Computer Vision*, vol. 50, no. 3, pp. 271-293, December, 2002. Article (CrossRef Link)

[9] D. Cremers, M. Rousson, and R. Deriche, "A review of statistical approaches to level set segmentation: integrating color, texture, motion and shape," *International Journal of Computer Vision*, vol. 72, no. 2, pp. 195–215, 2007. Article (CrossRef Link)

[10] C. Li, C.-Y. Kao, J. C. Gore, and Z. Ding, "Implicit active contours driven by local binary fitting energy," in *Proc. of IEEE Conf. on Computer Vision & Pattern Recognition*, pp. 1-7, June 17-22, 2007. Article (CrossRef Link)

[11] C. Li, R. Huang, Z. Ding, J. C. Gatenby, D. N. Metaxas, and J. C. Gore, "A level set method for image segmentation in the presence of intensity inhomogeneities with application to MRI," *IEEE Transactions on Image Process*, vol. 20, no. 7, pp. 2007-2016, April, 2011. Article (CrossRef Link)

[12] C. Li, J. C. Gore, and C. Davatzikos, "Multiplicative intrinsic component optimization (MICO) for MRI bias field estimation and tissue segmentation," *Magnetic Resonance Imaging*, vol. 32, no. 7, pp. 913-923, September, 2014. Article (CrossRef Link)

[13] S. Lankton and A. Tannenbaum, "Localizing region-based active contours," *IEEE Transactions on Image Process*, vol. 17, no. 11, pp. 2029-2039, September, 2008. Article (CrossRef Link)

[14] T. Brox and D. Cremers, "On local region models and a statistical interpretation of the piecewise smooth Mumford-Shah functional," *International Journal of Computer Vision*, vol. 84, no. 2, pp. 184-193, August, 2009. Article (CrossRef Link)

[15] K. Zhang, L. Zhang, K.-M. Lam, D. Zhang, "A level set approach to image segmentation with intensity inhomogeneity," *IEEE Transactions on Cybernetics*, vol.46, no. 2, pp. 546-557, March, 2016. Article (CrossRef Link)

[16] D. Chopp, "Computing minimal surface via level set curvature flow," *Journal of Computational Physics*, vol. 106, no. 1, pp. 77-91, May, 1993. Article (CrossRef Link)

[17] M. Sussman, P. Smereka, and S. Osher, "A level set approach for computing solutions to incompressible two-phase flow," *Journal of Computational Physics*, vol. 114, no. 1, pp. 146-159, September, 1994. Article (CrossRef Link)

[18] D. Peng, B. Merriman, S. Osher. H. Zhao, and M. Kang, "A PDE-based fast local level set method," *Journal of Computational Physics*, vol. 155, no. 2, pp. 410-438, November, 1999. Article (CrossRef Link)

[19] C. Li, C. Xu, C. Gui, and M. D. Fox, "Level set evolution without re-initialization: A new variational formulation," in *Proc. of IEEE Conf. on Computer Vision & Pattern Recognition*, pp. 430-436, June 20-25, 2005. Article (CrossRef Link)
[20] X. Xie, "Active contouring based on gradient vector interaction and constrained level set diffusion," *IEEE Transactions on Image Process*, vol. 19, no. 1, pp. 154-164, September, 2010. Article (CrossRef Link)
[21] C. Li, C. Xu, C. Gui, and M. D. Fox, "Distance regularized level set evolution and its application to image segmentation," *IEEE Transactions on Image Process*, vol. 19, no. 12, pp. 3243-3254, August, 2010. Article (CrossRef Link)
[22] K. Zhang, L. Zhang, H. Song, and D. Zhang, "Reinitialization-free level set evolution via reaction diffusion," *IEEE Transactions on Image Process*, vol. 22, no. 1, pp. 258-271, January, 2013. Article (CrossRef Link)
[23] Y. Duan, H. Chang, W. Huang, J. Zhou, Z. Lu, and C. Wu, "The L0 regularized Mumford-Shah model for bias correction and segmentation of medical images," *IEEE Transactions on Image Process*, vol. 24, no. 11, pp. 3927-3938, November, 2015. Article (CrossRef Link)
[24] H. Chang, W. Huang, C. Wu, S. Huang, C. Guan, S. Sekar, K. K. Bhakoo, and Y. Duan, "A new variational method for bias correction and its applications to rodent brain extraction," *IEEE Transactions on Medical Imaging*, vol. 36, no. 3, pp. 721-733, March, 2017. Article (CrossRef Link)
[25] M. N. Ahmed, S. M. Yamany, N. Mohamed, A. A. Farag, and T. Moriarty, "A modified fuzzy C-means algorithm for bias field estimation and segmentation of MRI data," *IEEE Transactions on Medical Imaging*, vol. 21, no. 3, pp. 193-199, March, 2002. Article (CrossRef Link)
[26] S. C. Chen, and D. Q. Zhang, "Robust image segmentation using FCM with spatial constrains based on new kernel-induced distance measure," *IEEE Transactions on Systems Man, Cybernetics Society*, vol. 34, no. 4, pp. 1907-1916, August, 2004. Article (CrossRef Link)
[27] K. S. Chuang, H.-L. Tzeng, S. Chen, J. Wu, and T.-J. Chen, "Fuzzy C-means clustering with spatial information for image segmentation," *Computerized Medical Imaging and Graphics*, vol. 30, no. 1, pp. 9-15, January, 2006. Article (CrossRef Link)
[28] D. W. Shattuck, S. R. Sandor-Leahy, K. A. Schaper, D. A. Rottenberg, and R. M. Leahy, "Magnetic resonance image tissue classification using a partial volume model," *Neuroimage*, vol. 13, no. 5, pp. 856-876, May, 2001. Article (CrossRef Link)
[29] B. Likar, M. A. Viergever, and F. Pernus, "Retrospective correction of MR intensity inhomogeneity by information minimization," *IEEE Transactions on Medical Imaging*, vol. 20, no. 12, pp. 1398-1410, December, 2001. Article (CrossRef Link)

Yanjun Peng received his Dr. degree in march, 2004. He joined the Department of Computer Science, Shandong University of science and technology, Qingdao, China, in 1996, where he was promoted to professor in 2010. His main research interests include medicine visualization, virtual reality, and image processing.

Yingran Ma received his M.S. degree in computer application technology from Shandong University of science and technology, Qingdao, China, in 2017. He is currently in his doctor degree acquisition in computer multimedia technology. His research interests include image processing, medical imaging and neural networks.